Achieving sub-Rayleigh resolution via thresholding

Sara Mouradian,[1,*] **Franco N. C. Wong,**[1] **and Jeffrey H. Shapiro**[1]

[1]*Research Laboratory of Electronics, Massachusetts Institute of Technology, Cambridge, Massachusetts 02139, USA*

[*]*smouradi@mit.edu*

Abstract: Diffraction from a finite-diameter entrance pupil imposes the Rayleigh bound on the spatial resolution achievable by a conventional imaging system. We demonstrate resolution beyond this limit through unstructured scanning of a focused laser beam across an object together with dynamic application of a threshold N less than the maximum count level $N_{\max}$. Experimental results show sub-Rayleigh resolution enhancement by a factor of $[\ln(N_{\max}/N)]^{1/2}$.

OCIS codes: (100.6640) Superresolution; (100.2980) Image enhancement.

References and links

1. Lord Rayleigh, "Investigations in optics with special reference to the spectroscope," Phil. Mag. **8,** 261–274 (1879).
2. C. M. Sparrow, "On spectroscopic resolving power," Astrophys. J. **44,** 76–86 (1916).
3. A. N. Boto, P. Kok, D. S. Abrams, S. L. Braunstein, C. P. Williams, and J. P. Dowling, "Quantum interferometric optical lithography: Exploiting entanglement to beat the diffraction limit," Phys. Rev. Lett. **85,** 2733–2736 (2000).
4. J. P. Dowling, "Quantum optical metrology—the lowdown on high-N00N States," Contemp. Phys. **49,** 125–143 (2008).
5. V. Giovannetti, S. Lloyd, L. Maccone, and J. H. Shapiro, "Sub-Rayleigh-diffraction-bound quantum imaging," Phys. Rev. A **79,** 013827 (2009).
6. M. Tsang, "Quantum imaging beyond the diffraction limit by optical centroid measurements," Phys. Rev. Lett. **102,** 253601 (2009).
7. K. Wang and D.-Z. Cao, "Subwavelength coincidence interference with classical thermal light," Phys. Rev. A **70,** 041801(R) (2004).
8. P. R. Hemmer, A. Muthukrishnan, M. O. Scully, and M. S. Zubairy, "Quantum lithography with classical light," Phys. Rev. Lett. **96,** 163603 (2006).
9. S. J. Bently and R. W. Boyd, "Nonlinear optical lithography with ultra-high sub-Rayleigh resolution," Opt. Express **12,** 5735–5740 (2004).
10. S. W. Hell, J. Soukka, and P. E. Hänninen, "Two- and multiphoton detection as an imaging mode and means of increasing the resolution in far-field light microscopy: A study based on photon-optics," Bioimaging **3,** 64–69 (1995).
11. A. J. Pearlman, A. Ling, E. A. Goldschmidt, C. F. Wildfeuer, J. Fan, and A. Migdall, "Enhancing image contrast using coherent states and photon number resolving detectors," Opt. Express **18,** 6033–6039 (2010).
12. D. Semwogerere and E. R. Weeks, "Confocal microscopy," in *Encyclopedia of Biomaterials and Biomedical Engineering*, G. E. Wnek and G. L. Bowlin, eds. (Taylor & Francis, 2005), pp. 705–714.
13. A. Pertsinidis, Y. Zhang, and S. Chu, "Subnanometre single-molecule localization, registration and distance measurements," Nature **466,** 647–651 (2010).
14. F. Guerrieri, L. Maccone, F. N. C. Wong, J. H. Shapiro, S. Tisa, and F. Zappa, "Sub-Rayleigh imaging via N-photon detection," Phys. Rev. Lett. **105,** 163602 (2010).

#139824 - $15.00 USD Received 20 Dec 2010; revised 23 Feb 2011; accepted 27 Feb 2011; published 8 Mar 2011

1. Introduction

In an ideal imaging system, the wavelength of the imaging light is the only limitation on the minimum resolvable feature size. However, as light passes through a finite aperture, the wavefront is modified and this modification is propagated to the image plane, forming a distorted image. This is diffraction. For instance, the intensity pattern created at the image plane by a laser focused at the object plane is not a point, but rather the Airy disk function due to diffraction through the finite aperture of the lens between the object and image plane. The image of an extended object is the convolution of the imaging system's point-source response with the object's overall transmissivity (reflectivity) pattern for imaging in transmission (reflection). It follows that any limits on the resolution of two closely-spaced point objects transfer directly to limitations on the resolution of an extended object's image.

The standard criterion for the resolution of two point-like objects is the Rayleigh limit. In 1879, Lord Rayleigh stated that two point-like objects can be resolved only if their separation projected onto the image plane is larger than the distance from the peak to the first null point of the Airy disk created by a single point source [1]. The minimum resolvable separation at the image plane is given by

$$R = \frac{0.61\lambda D_0}{R_{\mathrm{A}}} M, \tag{1}$$

where λ is the illumination wavelength, D_0 is the distance from the object plane to the radius-R_{A} entrance pupil that causes the diffraction, and M is the imager's magnification factor. Another notable limit is the Sparrow bound—the distance at which the two Airy disks overlap to form an intensity pattern with just a single peak. [2]. An imaging system whose spatial resolution capability exceeds these limits would be useful in many diverse applications, such as laser radar and biomedical microscopy.

1.1. Previous work

Many proposals for achieving increased resolution have relied on nonclassical light, such as Fock states or path-entangled states. These states provide sub-optical-wavelength diffraction patterns in N-photon coincidence detection that, in turn, afford resolution beyond limits imposed by the imaging wavelength [3–5]. Tsang demonstrated that N-fold resolution enhancement is possible with a multiphoton counting array and post-processing [6], suggesting that complicated N-photon coincidence detection is not necessary for achieving enhanced resolution. Although effective in principle, the preceding strategies are difficult to implement because the necessary photon states are challenging to create and extremely sensitive to loss.

The impracticality of generating and manipulating the quantum states needed for improved resolution has led several groups to investigate methods that employ conventional (classical-state) illumination. The classical correlation of a thermal light source has been shown to lead to sub-wavelength two-slit interference patterns—similar to those obtained with entangled-beam light sources—when joint intensity measurements are made at symmetrically displaced positions [7]. Coherent (laser) light can also produce sub-wavelength interference patterns with wave-vector correlation and frequency-selective multiphoton detection that uses Doppleron-type resonances [8]. These quantum-enhanced and classical techniques utilize correlations to achieve sub-wavelength resolution in an imaging system that is not diffraction limited.

However, he minimum resolvable feature size imposed by diffraction through finite elements in the imaging system (e.g. the Rayleigh and Sparrow limits) is much larger than the limits imposed by the imaging wavelength. Several classical techniques have been suggested to surpass these diffraction bounds. They rely on multiphoton detection, point-by-point illumination, post-processing, or combinations thereof. Bently and Boyd showed that lithographic measurements with N-photon-absorbing material—simulated by Nth harmonic generation followed by

#139824 - $15.00 USD Received 20 Dec 2010; revised 23 Feb 2011; accepted 27 Feb 2011; published 8 Mar 2011

photodetection with a charge-coupled device (CCD)—can, in principle, achieve significant resolution enhancement beyond the Rayleigh limit [9]. In the biomedical field, Hell *et al.* proposed N-photon-detection microscopy for enhanced imaging of fluorescent molecules [10]. N-photon detection has the effect of taking the Nth power of an ordinary intensity image, so that its peaks and dips are accentuated, thus yielding higher contrast. This has been recently demonstrated with photon-number resolving detectors [11]. However, these authors note that applying N-photon detection to conventional full-object-illumination imaging cannot surpass the Sparrow limit, as there are no dips or features to accentuate [11].

Point-by-point object illumination is employed in confocal scanning microscopy, a common biomedical-imaging strategy [12]. A biological sample is scanned with a tightly focused laser which causes the fluorescence of biological markers. A pinhole is placed at the image plane to limit the radius of the light reaching the detector. This method improves resolution by removing the information not at the center of the Airy disk. Though this method increases resolution, it has certain limitations. To obtain the increase in resolution, the light reaching the image plane is drastically reduced by the pinhole. Thus, the imaging light must be powerful to achieve an acceptable signal-to-noise ratio. Also, for best results, the center of the pinhole should always match exactly the center of the Airy disk. Thus, the pinhole at the image plane must follow the movement of the imaging beam exactly. This is feasible in microscopy where the distance between the object and image planes is small. This would be much more difficult in other applications where the object and image planes are well separated, and where scattering may occur.

Increased resolution can also be achieved with prior knowledge of the object to inform post-processing, e.g., Pertsinidis *et al.* recently demonstrated subnanometer resolution in imaging two adjacent fluorescent molecules [13]. By taking advantage of the highly symmetric fluorescence pattern of each molecule, and using servo control to actively stabilize the imaging system, they were able to determine the centroid location with 0.5 nm resolution. However, this prior-knowledge technique is only applicable in special situations.

To surpass the Sparrow limit for imaging arbitrary extended objects, Giovannetti *et al.* [5] proposed a technique that combines point-by-point illumination with N-photon detection to yield significant resolution enhancement. A striking advantage of their technique is that the scanning can be completely unstructured, as long as it covers the object of interest, thus obviating the need for any prior knowledge. The concept was recently demonstrated experimentally by Guerrieri *et al.* [14] using focused-laser illumination and image capture with a single-photon avalanche detector (SPAD) array. The experiment was performed with low-brightness illumination, i.e., a maximum average number of detected photons per pixel per exposure of $N_{\max} = 15$. Their experiment yielded sub-Sparrow resolution by imposing a threshold N greater than $N_{\max}$ at each pixel of the detection array. At this low light level, shot noise is quite significant so that thousands of image frames had to be averaged at every illumination location. The experimental resolution enhancement was found to be in agreement with the theoretical prediction of $(N - N_{\max})^{1/2}$ [14].

2. Focused illumination and thresholding strategy

In this work, we extend the results of Guerrieri *et al.* by modifying their technique of focused scanning and thresholding to be compatible with CCD-array detection. We are able to use a standard imaging device instead of the SPAD array because we employ a high-brightness source that yields collected light sufficiently strong to be detected conventionally and to neglect Poisson shot-noise when it is tightly focused on the object plane. Hence a single CCD image captures all information available from the illuminated region making multi-frame averaging unnecessary.

#139824 - $15.00 USD Received 20 Dec 2010; revised 23 Feb 2011; accepted 27 Feb 2011; published 8 Mar 2011

To quantify the improvement from this technique, we approximate the Airy disk by a Gaussian whose peak value $N_{\max}$ and $1/e^2$ half-width σ match those of the Airy disk. This is a common approximation, and one that allows a closed-form expression for the effect of a threshold. σ is determined completely by the imaging setup, and is found by minimizing the difference between the Gaussian approximation and the actual intensity pattern for the central portion of the acquired point-illuminated image. Thus, for a given image we approximate the counts near the center with a Gaussian distribution given by

$$N(x) = N_{\max} e^{-x^2/\sigma^2}, \tag{2}$$

where x is the distance from the peak of the point-illuminated image. We then pick the new width σ_N according to the following procedure. A smaller σ_N increases the resolution of the final post-processed image, but it has a lower limit that is set by the size of the CCD pixels. However, a smaller σ_N will also lead to a longer image-acquisition time because a larger number of finer-scale scans is needed to generate the whole image. Thus, the choice of σ_N depends on the needs of the imaging measurements in terms of resolution and acquisition times. For a given $x = \sigma_N$, Eq. (2) yields the required pixel-count threshold $N(\sigma_N)$ and hence the ratio $N(\sigma_N)/N_{\max}$. In the computer post-processing code we set this ratio according to the desired width σ_N (e.g., $N(\sigma_N)/N_{\max} = 0.939$ for black and white imaging). Thus, for a given threshold N, we obtain a reduced half-width given by

$$\sigma_N = \sigma \sqrt{\ln\left(\frac{N_{\max}}{N}\right)}, \tag{3}$$

so long as this value exceeds the resolution limits set by the CCD pixel size and the beam waist of the focused-beam illumination at the object. This process is shown in Fig. 3(a). For gray-scale objects, light intensity will vary for each imaged point. Setting the threshold N as a function of $N_{\max}$ (by setting the ratios instead of the absolute value of N) for each illumination point allows the reduced point size to be constant over all regions, and allows the effortless recording of these changes in intensity. Thus, setting the threshold dynamically enables imaging of gray-scale objects.

3. Experiments

3.1. Setup

Figure 1 is a schematic of our experimental setup for demonstrating the sub-Rayleigh imaging technique described above. The illumination source was a 532-nm-wavelength laser that was focused to a beam waist of 20 μm at the object. The focused spot was scanned manually over the object by adjusting the angle of a flat mirror. The $M = 1$ imaging system was located 110 cm from the object plane, and consisted of a diffraction-limited focusing lens, a relay imaging lens, and a CCD array. The focusing lens' focal length was 25 cm and it could be covered with a 1-mm-radius aperture to impose a stringent diffraction limit. The distance D_m between the scan mirror and the object was large enough to ensure uniform-brightness illumination at the imaging aperture over the entire area of interest at the object plane.

Two targets were imaged in transmission to demonstrate resolution enhancement in both opaque vs. transparent imaging and gray-scale imaging. In the former case we used the Group 2, Element 2 portion of the standard U.S. Air Force (USAF) resolution target, which consists of 3 alternating 111-μm-wide, 555-μm-high opaque and transparent stripes, as indicated in Fig. 2(a). The Rayleigh bound for our $M = 1$ imaging system with the 1-mm-radius aperture in place was calculated to be 357 μm from Eq. (1), which is 3.2$\times$ larger than the 111-μm feature

#139824 - $15.00 USD Received 20 Dec 2010; revised 23 Feb 2011; accepted 27 Feb 2011; published 8 Mar 2011

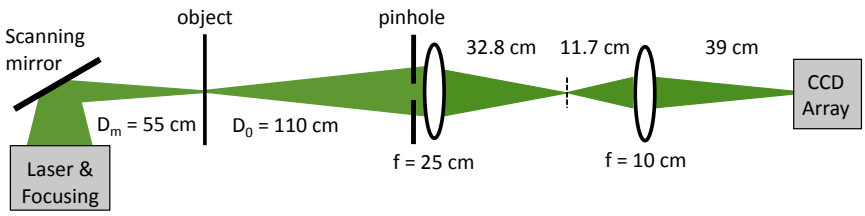

Fig. 1. Experimental setup for CCD-based sub-Rayleigh imaging system.

size at the image plane. For gray-scale imaging, a four-region section of an ISO-21550 dynamic range film target was used, as shown in Fig. 2(b). The regions labeled 3, 5, 6, and 9 had 77.6%, 40.4%, 20.9%, and 1.56% transmissivities, respectively.

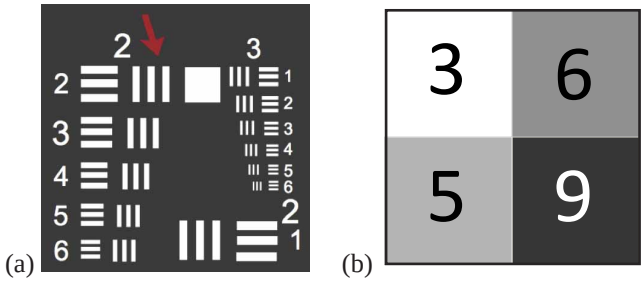

Fig. 2. (a) USAF resolution target: red arrow indicates area of interest in Group 2, Element 2, with stripe width of 111 μm. (b) Section of an ISO-21550 dynamic range film target for gray-scale imaging, with specified transmissivities of 77.6%, 40.4%, 20.9%, 1.56% for regions 3, 5, 6, and 9, respectively.

We used a 12-bit-output CCD array (Basler model piA1600-35gm) whose $7.4 \times 7.4\,\mu\text{m}^2$ pixel size was small in comparison to both the object feature size and the illumination's beam waist at the object. The CCD had a dark noise of $\sim$2 counts for our typical 50 μs exposure time, and we confirmed the manufacturer's $\sim$13 photons/bit conversion-efficiency specification in our own tests. All processing code was written in C#, building upon a library provided by Basler. Image formation proceeded as follows. An initial image was recorded and the intensity pattern was fit to a gaussian distribution and the standard deviation, σ was recorded. Then, the desired new width, σ_N was set. Prior to any measurements an all-zero image of the object region was stored. When an image frame was acquired for a single exposure at a particular illumination location. The threshold was set according to N_{max} and the chosen σ_N. Pixels with count values at or above the threshold retained their counts while all others were set to zero. Then the stored image was updated by incorporation of the above-threshold pixels from the processed frame. This process was repeated at every point covered by the scanning pattern, building the final image one point at a time.

3.2. Measurements and results

Figure 3(a) illustrates the effect of thresholding on the diffraction-limited image of a focused spot (20 μm radius) at the object plane without a target in place. The black curve is a cross section through the center of the raw image obtained in a single CCD measurement frame

#139824 - $15.00 USD Received 20 Dec 2010; revised 23 Feb 2011; accepted 27 Feb 2011; published 8 Mar 2011

with a maximum count value $N_{\max} = 1050$. Note that σ, the $1/e^2$ half-width of the Gaussian approximation of the Airy disk, is ~20 pixels. We applied two threshold values, $N = 800$ (red dashed line) and 1000 (blue dashed line). All pixels with values below N were set to zero (the initialized value for each pixel) and stored. Associated with each threshold in Fig. 3(a) are two vertical lines indicating the full widths $2\sigma_N$ of the modified point-source image, given by Eq. (3). As the threshold increases toward $N_{\max}$, we can obtain a dramatic reduction in the point-source image size, as shown in Fig. 3(b). Moreover, because the initial point-source image is highly symmetric about its peak, the post-processed image suffers no appreciable shift in the location of the center relative to that of the raw (unprocessed) image.

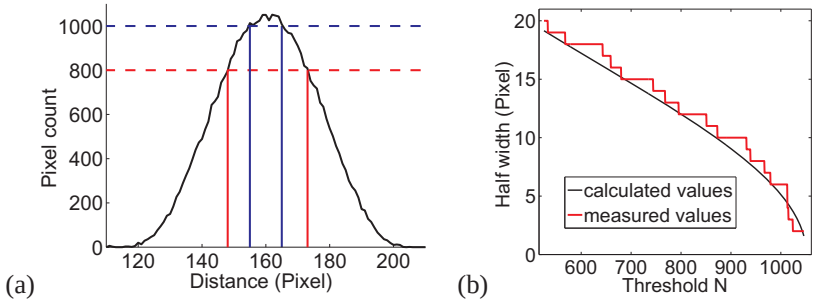

Fig. 3. (a) Cross section through the center of a diffraction-limited image (black curve) of a point source. The dashed lines indicate two threshold values, N = 800 (red) and N = 1000 (blue), that yield reduced widths—after sub-threshold pixel values are set to zero—which are bounded by the two corresponding vertical lines. (b) Plot of half-widths σ_N (in pixels) as a function of the threshold value N for the image in (a).

We first imaged the USAF target indicated in Fig. 2(a) and described in section 3.1. First, we performed conventional, full-object illumination imaging both without (Fig. 4(a)) and with (Fig. 4(b)) a 1-mm-radius aperture at the entrance to the imaging system as seen in Fig. 1. The illumination beam was expanded to a radius of 3 mm to cover the entire area of interest at the object plane. Without the aperture, the image is well-resolved and the three stripes have the expected width of 111 μm (15 pixels). With the aperture, the Raylieigh limit at the image plane is 357 μm (48 pixels) as given by Eq. (1). This is much larger than the stripes, and thus they are not resolved.

We then imaged the USAF target using focused scanning and threshold application as described in section 3.1. Figures 4(c) and (d) are the images obtained with the focused illumination and thresholding technique under high-power and low-power illumination, respectively. Our imaging system had $1/e^2$ half-width $\sigma = 20$ pixels, and we chose $\sigma_N = 5$ pixels for a resolution enhancement factor σ/σ_N of 5. To achieve σ_N of 5 pixels (37 μm), we set the threshold $N = 0.939N_{\max}$, according to Eq. (3). Under high power illumination, $N_{\max}$ was typically ~1000 counts per pixel with an exposure time of 50 μs. The full image was built point-by-point as the illumination beam was scanned over the image. The final image obtained under high power illumination is shown in Fig. 4(c). The three stripes of the USAF target are clearly resolved using our technique.

The increased resolution of our technique is tested at the boundaries between opaque and transparent areas where the light diffracts at the object plane as well as at the imaging system. The Airy disks of two adjacent illumination points will overlap. At the boundaries, the maximum values of the two points will be different. Because new non-zero pixel values always replace old pixel values in updating the stored image as described in Sec. 3.1, the final intensity

#139824 - $15.00 USD Received 20 Dec 2010; revised 23 Feb 2011; accepted 27 Feb 2011; published 8 Mar 2011

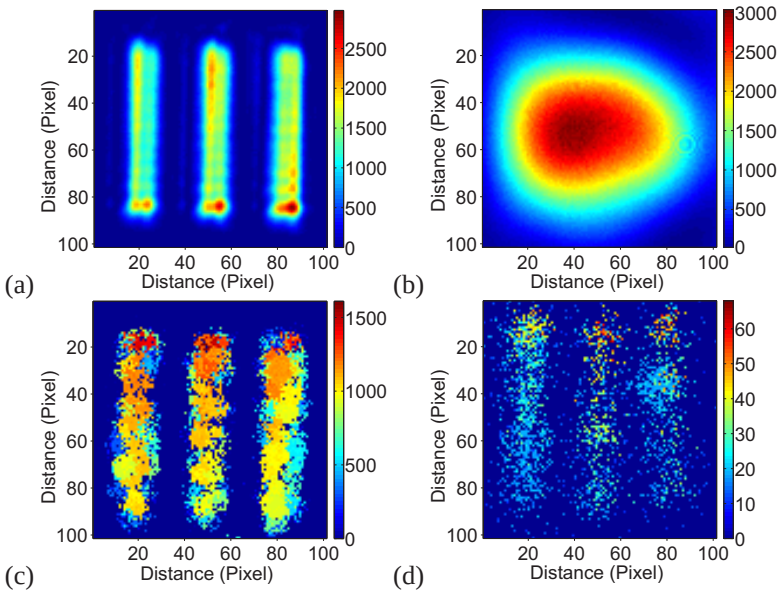

Fig. 4. Images of USAF resolution target using different methods (and incident powers). (a) Conventional full-object illumination with no aperture (30 μW). (b) Diffraction-limited conventional imaging with 1-mm-radius aperture (150 μW). (c) Sub-Rayleigh imaging with focused scanning and thresholding at high power (30 μW). (d) Sub-Rayleigh imaging with focused scanning and thresholding at low power (3.5 μW).

of the overlap region depends on the order of scanning—if the opaque point is imaged first (last), the overlap will be brighter (dimmer). This causes the slight jaggedness (of the order of $\sigma = 5$ pixels) and intensity variation along the edges of the stripes. This is unavoidable because the beam has a finite size at the object plane and thus diffraction will always occur near sharp edges. However, the uneven edges can be reduced by either decreasing the beam waist or by increasing the threshold to obtain a smaller σ_N. Smoothing the edges by either method would require scanning at a finer scale and therefore increase image-acquisition time.

To evaluate sub-Rayleigh image formation under weak illumination, we reduced the illumination power and made measurements with the room lights turned on. The average background count without illumination, for 50 μs exposure time, was $\sim$20 counts per pixel. With illumination, $N_{\max}$ was $\sim$60 counts per pixel giving a signal-to-noise ratio of only two. Even so, the three stripes are still clearly discernible with scanned focused illumination and thresholding, although they are of course much fainter than under bright illumination. The more saturated portions of Fig. 4(d) were covered more heavily by the scan pattern we employed. From this, we can infer that increasing the acquisition time in the weak illumination scenario increases the contrast and signal-to-noise ratio of the final image. At even lower powers, we enter the regime described by Guerrieri *et al.* as Poisson shot-noise becomes relevant so that the SPAD array approach [14] would be necessary to obtained resolved images.

So far, we have demonstrated that focused illumination, thresholding, and CCD detection combine to provide resolution enhancement in accord with Eq. (3) for opaque and transparent objects observed in transmission. Our method has two significant advantages: only one image is necessary at each point, and the threshold value can be set independently and dynamically for each individual illumination point based entirely on the maximum count value for that

#139824 - $15.00 USD Received 20 Dec 2010; revised 23 Feb 2011; accepted 27 Feb 2011; published 8 Mar 2011

image. Dynamic thresholding implies that gray-scale objects can be imaged with our procedure, increasing the scope of potential applications.

As a preliminary demonstration of this capability, we performed additional imaging experiments, using the gray-scale test film shown in Fig. 2(b) as the target. Figure 5(a) is the conventional, full-object-illumination image of this gray-scale test film without the 1-mm-radius aperture. Because the purpose of our gray-scale imaging measurement was to demonstrate the ability to replicate intensity variations and not to achieve high resolution of the boundaries between different regions, we decreased the threshold thus increasing the post-processed spot at the image plane and reducing the time needed for full scanning coverage of the object. This led to the spotted patterns and indistinct boundaries shown in Fig. 5(b). However, even with the lower threshold, Fig. 5(b) shows that focused scanning with the pinhole in place provides an image of the four regions whose clarity is comparable to that of the conventional no-aperture image in Fig. 5(a).

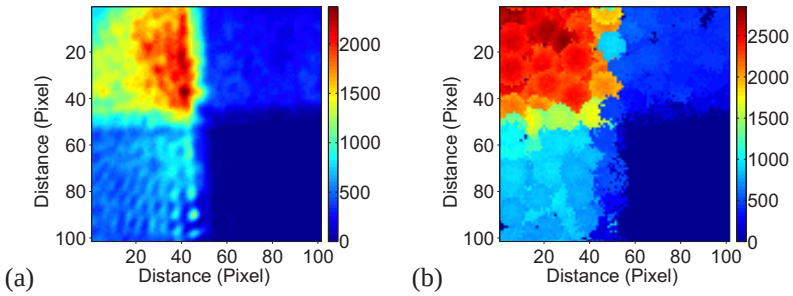

Fig. 5. Gray-scale target imaged with (a) conventional full-object illumination without aperture, and (b) focused scanning with a 1-mm-radius aperture and thresholding.

From the gray-scale sub-Rayleigh image in Fig. 5(b) we inferred the relative transmissivities of the four labeled target regions in Fig. 2(b). The gray-scale test film's specifications were as follows: a ratio of 1.9 between regions 3 and 5, 1.9 between regions of 5 and 6, and 13.4 between regions of 6 and 9. In comparison, the corresponding values we inferred from our sub-Rayleigh image were 2.5, 2.2, and 22. The first two ratios (between regions 3 and 5, and regions 5 and 6) are in good agreement with the specifications. The slightly larger difference ($\sim$60%) for the ratio between regions 6 and 9 is partly due to the fact that very little light was transmitted through region 9 and background counts dominated the region-9 measurement. In addition, the aperture might not have been centered relative to the target, so that some of the transmitted light from different regions did not pass through the focusing lens. We should point out that the measured ratio of 22 between regions 6 and 9 for the focused-illumination image in Fig. 5(b) is in closer agreement with the measured ratio of 26 for the full-object-illumination image in Fig. 5(a). Thus it is clear that the thresholding technique works very well for imaging gray-scale objects.

4. Conclusion

We have demonstrated that focused scanning plus dynamic application of a threshold for each illumination point can increase resolution beyond the Rayleigh and Sparrow diffraction limits under both high-power and low-power illumination. Indeed, the use of focused scanning is essential for enhancing the resolution well below the Sparrow limit, which cannot be achieved by post-processing full-object-illumination data. The resolution improvement in our technique is bounded only by the pixel size of the CCD camera and the illumination's beam waist at

#139824 - $15.00 USD Received 20 Dec 2010; revised 23 Feb 2011; accepted 27 Feb 2011; published 8 Mar 2011

the object plane. The dynamic nature of setting the threshold for each exposure facilitates sub-Rayleigh imaging of gray-scale objects without modification of the implementation or the post-processing methodology, an effect difficult to achieve with previous sub-Rayleigh imaging suggestions. Moreover, the final point size at the image plane can be adjusted easily to trade resolution for imaging speed as desired. The time needed to image an entire object can also be greatly decreased if multiple lasers are used to illuminate many points at once. The resolution enhancement for each illuminated point would be preserved so long as the illumination points are separated far enough that the dip between their Airy disks falls below the imposed threshold.

In the experiment presented here, the object was imaged in transmission. However, we believe that the technique would work in reflection as well. This opens up the possibility of color imaging. To perform sub-Rayleigh color imaging, the single frequency laser is replaced by a broadband coherent light source and the detector is chosen to detect the red, green, and blue components of the return signal, which is a standard capability of CCD arrays. The response to a point then becomes three Airy disks (red, green, blue), of different amplitudes, which can be subjected to different thresholds. Thus, color imaging is analogous to the gray-scale imaging we have demonstrated here. We believe that our sub-Rayleigh imaging work based on focused illumination, thresholding, and CCD detection can be applied to a wide range of imaging situations.

Acknowledgment

This work was supported by the U.S. Army Research Office MURI Grant No. W911NF-05-0197.

#139824 - $15.00 USD Received 20 Dec 2010; revised 23 Feb 2011; accepted 27 Feb 2011; published 8 Mar 2011